HEMT Average Temperature Determination Utilizing Low-Power Device Operation

M. Florovič, J. Kováč, Jr., A. Chvála, J. Kováč, *Member, IEEE*,
J.-C. Jacquet, S. L. Delage, *Member, IEEE*

***Abstract*—The modified thermal device model was adapted to determine the channel temperature of the AlGaN/GaN HEMT operating under pulsed and quasi-static conditions. The differential analysis of the isothermal and thermal part of the resulting current, as well as ambient temperature variation, is utilized to determine the average channel temperature. Ambient temperature increases in the device operating range is required under low-power operation only, while under high-power operation the thermal stress of the device is significantly reduced due to small ambient temperature variation. In addition, trapping phenomena incorporation is demonstrated to obtain more accurate results utilizing the HEMT threshold voltage shift and transconductance. For experimental verification of the thermal model, $Al_{0.25}Ga_{0.75}N$/GaN HEMT electrical properties are investigated. Experimentally verified results are in a good agreement with numerical simulations.**

***Index Terms*—AlGaN, average channel temperature, charge trapping, FET, GaN, HEMT.**

I. INTRODUCTION

THE high mobility combined with a high carrier density in two-dimensional electron gas (2DEG) in gallium nitride (GaN)-based wide bandgap structure gives an opportunity to fabricate the advanced electrical devices like high electron mobility transistors (HEMTs) exhibiting superior properties in the field of high-power, temperature, frequency, and microwave applications [1], [2], [3]. However, high operating voltage resulting in a high local electric field and dissipated power density bringing device self-heating have an impact on the device reliability although those negative phenomena are nowadays suppressed by advanced horizontal and vertical device design such as substrates with high thermal conductance utilization [4], [5], [6].

Besides plenty of experimental methods to estimate device operation temperature like Raman spectroscopy or interferometric mapping [7], [8] electrical measurements utilizing low-power operating regime including external heating [9], [10] were employed taking advantage from specific electro-thermal device properties if the active device itself is concerned as temperature sensor [11], [12].

Here isothermal and thermal processes are required to be sorted to obtain relevant results. Besides that, the device reliability plays a significant role during the measurements when ambient temperature variation along the operating temperature range is required. Moreover, pulse measurements suffer from finite applied voltage increase and real device electrical parasitic capacitance. Therefore, low-power measurements are utilized, the quasi-static and pulse measurements relation is highlighted, and isothermal current at the beginning of the pulse is estimated. The theoretical considerations are possible to be applied for ungated or gated field-effect transistor (FET) structure neglecting gate current. In this work, they are practically utilized to acquire AlGaN/GaN HEMT channel average temperature based on hypothetic situation demonstrated by infinite channel thermal conductance in the active device area where power density inside plays no role to avoid thermal gradient calculations. The obtained experimental results under low-power and high-power operations are compared taking average temperature meaning into account and subsequently verified by temperature profile simulations.

II. THEORY

The same temperature is supposed to be reached along the device active area corresponding to the average temperature T_A [13]. The resultant current I_{DS} change between two ohmic contacts of gated or ungated FET structure is described by thermal current change dI_T, assigned to dT_A including thermal thermal change of carrier concentration, velocity and mobility, and isothermal current change dI_E at defined time interval dt. Isothermal current change $dI_E = dI_{\mathrm{VE}} + dI_{\mathrm{TE}}$ is related to dI_{VE} caused by immediate applied gate voltage V_{GS} or drain voltage V_{DS} change including parasitic electric capacitance charge. The term dI_{TE} corresponds to trapped charge isothermal variation [13]. Trapped charge variation under the

---

Manuscript received 29 July 2022; accepted 17 August 2022. Date of publication 5 September 2022; date of current version 22 September 2022. This work was supported in part by the ECSEL Joint Undertaking Project 5G_GaN2 under Agreement 783274, in part by the Projects of Scientific Grant Agency [Vedecká Grantová Agentúra (VEGA)] under Grant 1/0733/20, and in part by Slovak Research and Development Agency, Ministry of Education, Science, Research and Sport, Slovak Republic under Grant APVV-21-0365. The review of this article was arranged by Editor M. Hua. *(Corresponding author: M. Florovič.)*

M. Florovič, J. Kováč, Jr., A. Chvála, and J. Kováč are with the Faculty of Electrical Engineering and Information Technology, Institute of Electronics and Photonics, Slovak University of Technology, 81219 Bratislava, Slovakia (e-mail: martin.florovic@stuba.sk; jaroslav_kovac@stuba.sk; ales.chvala@stuba.sk; jaroslav.kovac@stuba.sk).

J.-C. Jacquet and S. L. Delage are with III-V Lab, 91460 Marcoussis, France (e-mail: jean-claude.jacquet@3-5lab.fr; sylvain.delage@3-5lab.fr).

Color versions of one or more figures in this article are available at https://doi.org/10.1109/TED.2022.3200630.

Digital Object Identifier 10.1109/TED.2022.3200630

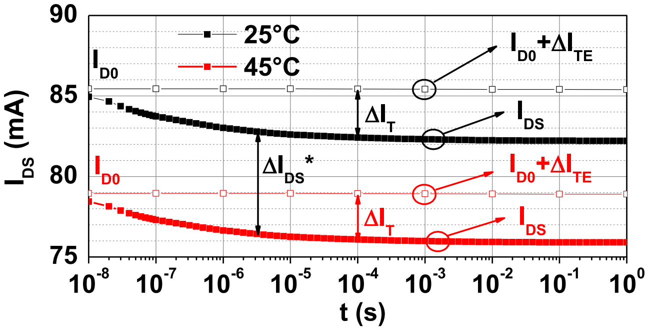

Fig. 1. Measured current I_{DS}, initial current I_{D0}, isothermal current $I_{D0} + \Delta I_{\mathrm{TE}}$ at $V_{\mathrm{DS}} = 2$ V.

gate is linearly assigned to threshold voltage V_{TH} shift of gated structure because of virtual gate superposition [14]. The correct dI_T and dI_E acquisition during time interval dt is requisite for proper dT_A determination.

Ambient temperature and zero dissipated power along the device active area are the initial conditions. After rectangular V_{GS} or V_{DS} pulse application at the zero time, the resultant current $I_{D0} = I_{\mathrm{DS}}(0)$ is reached supposing negligible rising time in comparison to thermal time constants.

A. Low-Power Operation Condition

Coming out from T_A definition [13] for rectangular voltage pulse for small power dissipation $P(t) = V_{\mathrm{DS}}(t)I_{\mathrm{DS}}(t)$ and inconsiderable $P(t)$ variation the thermal resistance $\Delta R_A(t, T_0) = T_A/P(t)$ is defined at time t and low-power ambient temperature T_{0L} utilizing $\Delta T_A = T_A - T_{0L}$. In the FET case, linear operating regime exhibits relatively low spatial deviation of the power dissipation and temperature distribution along the device active area.

The device investigated at two ambient temperatures T_{0L}, $T_{0L} + \Delta T_{0L}$ of relatively small difference ΔT_{0L} exhibits the active area differential temperature ΔT_A^* and differential current $\Delta I_{\mathrm{DS}}^* = k_T \Delta T_A^*$ resulting in $\Delta T_A/\Delta T_A^* = \Delta I_T/\Delta I_{\mathrm{DS}}^*$ utilizing $\Delta T_A = T_A - T_{0L}$ and $\Delta I_T \approx I_{\mathrm{DS}}(t) - I_{D0} - \Delta I_{\mathrm{TE}}(t)$ because of the same thermal coefficient k_T and relatively small $P(t)$ variation during low-power operation [13], [14] as illustrated in Fig. 1. Isothermal trapping phenomena are covered by the term ΔI_{TE}.

Therefore, R_A is possible to be calculated under low-power operation condition. The V_{GS} or V_{DS} step is required to be sufficiently high to acquire ΔI_T. Dissipated power difference $\Delta P^*(t) = V_{\mathrm{DS}} \Delta I_{\mathrm{DS}}^*(t)$ brings $\Delta\Delta T_A^* = T_{0L} + R_A(t, T_{0L})\Delta P^*(t)$. Subsequently, R_A is yielded as

$$\Delta R_A(t, T_{0L}) = \frac{\Delta T_{0L} I_T}{V_{\mathrm{DS}} \Delta I_{\mathrm{DS}}^*(t)} [I_{D0} + \Delta I_{\mathrm{TE}}(t)]^{-1}. \quad (1)$$

Dissipated power change $|\Delta P^*(t)| \ll \Delta T_{0L}/R_A(t, T_{0L})$ caused by ΔI_{DS}^* variation turns (1) into the simplified form possible to be utilized especially for low V_{DS} under low-power device operation

$$\Delta R_A(t, T_{0L}) = \frac{\Delta T_{0\mathrm{L}} I_T}{V_{\mathrm{DS}} \Delta I_{\mathrm{DS}}^*(t) I_{\mathrm{DS}}(t)}. \quad (2)$$

B. Average Temperature Estimation Possibilities

The ambient temperature T_{0H} for high-power operation is required to be distinguished from low-power operation ambient temperature T_{0L} for T_A recurrent calculations purposes in the way $T_{A,n} = T_{0H} + \sum_{k=1}^{n} \Delta T_{A,k}$ utilizing integer series coefficients k and n. The average temperature difference $\Delta T_{A,k}$ is linearly dependent on dissipated power or time variation at $T_{A,k} = T_{0L}$ utilizing $R_A(t_k, T_{A,k}) = R_A(t, T_{0L})$ or normalized thermal resistance $k_{R,k} = R_A(t_k, T_{A,k})/R_A(t_k, T_{0H})$ from low-power measurements.

Under the quasi-static state device operation, $R_A(t \to \infty, T_{A,k}) = R_{A\infty}(T_{A,k})$ is utilizing [15] resulting in

$$\Delta T_{A\infty,n} = T_{0H} + \sum\nolimits_{k=1}^{n} R_{A\infty}\left(T_{A,k}\right) P_k. \quad (3)$$

The T_A increase coming out from operation state time superposition results in $dT_A(t)/dt \approx P(t)dR_A(t, T_A)/dt$. This is applicable for rectangular pulse operation of small proportional $P(t)$ variation under high-power and low-power operation and results in

$$\Delta T_{A,n} = T_{0H} + \sum\nolimits_{k=1}^{n} \left[dR_A\left(t_k, T_{A,k}\right)/dt\right] P(t_k) t_k. \quad (4)$$

Although FET operating in the saturation regime exhibits eligible temperature gradient and strongly uneven power dissipation along the active area in comparison to linear regime, the proper T_A interpretation provides this method applicable.

C. Differential Average Temperature Calculation

To avoid T_A misinterpretation for the high-power V_{GS} or V_{DS} pulse response due to different high-power $R_A(t, T_A)$ and low-power $R_A(t, T_{0L})$ values at $T_A = T_{0L}$ caused by partially various heat flux spatial distribution along the device active area, the low-power operation is utilized to obtain $k_R(t, T_{0L}) = R_A(t, T_{0L})/R_A(t, T_{0H})$ only. The condition of similar normalized thermal resistance k_R for both cases is better fulfilled coming out from T_A definition [15].

The high-power I_{DS} time dependence is required to be obtained at two ambient temperatures of relatively small ambient temperature difference ΔT_{0H} corresponding to active area temperature difference ΔT_A^* and resultant current difference ΔI_{DS}^*. Subsequently, $dT_A = \Delta T_A^* dI_T/\Delta I_{\mathrm{DS}}^*$ is calculated utilizing thermal current contribution $dI_T = dI_{\mathrm{DS}} - dI_{\mathrm{TE}}$ during dt at t and T_A including isothermal trapping current contribution dI_{TE}.

The difference ΔT_{0H} results in $\Delta P^*(t) = V_{\mathrm{DSn}} \Delta I_{\mathrm{DS}}^*(t)$ and $\Delta\Delta T_A^* = [R_A(t, T_A)/R_A(t, T_{0H})]T_{0H} + [R_A(t, T_A)]\Delta P^*(t)$ [15], [16]. For thermal resistance and capacitance defined at T_{0H} the average temperature contribution $dT_{A0} = dT_A/k_R$, $\Delta T_{A0}^* = \Delta T_A^*/k_R$ are possible to be defined utilizing $\Delta T_{A0}^* = \Delta T_{0H} + R_A(t, T_{0H})\Delta P^*(t)$, $\Delta R_A(t, T_{0H}) = T_{A0}/P(t)$ coming out from linear $\Delta T_{A0} = T_{A0} - T_{0H}$ dependence versus dissipated power. Therefore, T_{A0} and T_A increase result in

$$dT_{A0} = \left[\Delta T_{0H} + R_A(t, T_{0H})\Delta P^*(t)\right] dI_T/\Delta I_{\mathrm{DS}}^* \quad (5)$$

$$dT_A = k_R(t, T_A) dT_{A0}. \quad (6)$$

The term $R_A(t, T_{0H})$ in (5) is estimated from the previous operating point. Recurrent calculations allow average

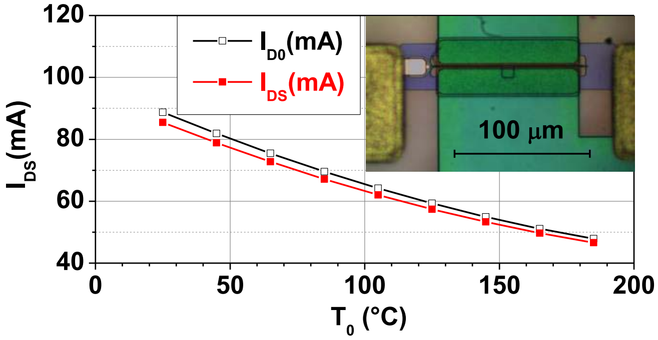

Fig. 2. Temperature dependence of measured current I_{DS} at $t \approx 1$ s and initial current I_{D0} at $V_{\mathrm{DS}} = 2$ V. (Inset: top view microscope image of investigated HEMT.)

temperature time dependence acquisition $T_{A0,n} = T_{0H} + \sum_{k=1}^{n} \Delta T_{A0,k}$ and $T_{A,n} = T_{0H} + \sum_{k=1}^{n} \Delta T_{A,k}$ using (5) as $\Delta T_{A0,k} = [\Delta T_{0H} + R_{A,k-1}(t, T_{0H})\Delta P_k^*(t)]\Delta I_{T,k}/\Delta I^*_{\mathrm{DS},k}$ and (6) as $\Delta T_{A,k} = k_{R,k}\Delta T_{A0,k}$ corresponding to Δt_k.

The condition $R_A(t, T_{0H})\Delta P^*(t) \ll \Delta T_{0H}$ and $|dI_{\mathrm{TE}}| \ll |dI_{\mathrm{DS}}|$ turns (5) into $dT_A = k_R \Delta T_{0H} dI_{\mathrm{DS}}/\Delta I^*_{\mathrm{DS}}$. However, the term $R_A(t, T_{0H})\Delta P^*(t)$ for high V_{DS} plays significant role in (5).

The recursive way of recurrent calculations starting at the end of long V_{GS} or V_{DS} pulse equivalent to quasi-static state and initial conditions $R_{A\infty}$ and $T_{A\infty}$ gives opportunity to avoid I_{D0} and $P(t)$ estimation at the beginning of the voltage pulse. On the other hand, dI_{TE} is possible to be neglected in (5) at the pulse beginning.

III. EXPERIMENTAL

A. Structure Design and Experimental Setup

The 14 nm $\mathrm{Al_{0.25}Ga_{0.75}N}$/1.5 nm AlN/1700 nm GaN/75 nm TBR heterostructure was grown by MOVPE on 70-μm-thick 4H-SiC substrate and top ohmic drain–source and gate contacts were formed by standard Au-based metallization to fabricate gated transmission line model (GTLM) $\mathrm{Al_{0.25}Ga_{0.75}N}$/GaN HEMT of width $w \approx 100$ μm with a gate of length $d_G \approx 0.15$ μm, the source to gate gap of length $d_{\mathrm{GS}} \approx 0.75$ μm and the drain to gate gap of length $d_{\mathrm{GS}} \approx 1.5$ μm [17] as shown in the inset of Fig. 2. The substrate backside Au contact soldered to 1-mm-thick CuMo leadframe makes possible to set investigated device in the open package placed on the Al thermal chuck preserved at a constant temperature.

Semiconductor parameter analyzer Agilent 4155C and controlled thermal chuck were utilized to acquire I_{DS} time response on V_{DS} pulse of amplitude 2 and 20 V keeping zero V_{GS}. The chuck temperature was set in the range 25 °C–185 °C to compare low-power and high-power methods based on ambient temperature and threshold voltage variation. Pulse measurements were done by utilizing pulse generator unit (PGU) as the 4155C extension unit. White LED illumination for one minute between measurements was utilized for the device recovery. The 3-D model incorporating device geometry, layout, and thickness of individual layers was employed in the 3-D thermal FEM simulations performed by Synopsys TCAD Sentaurus [18]. Material thermal conductivity and capacity values were obtained from the previous work and calibrated utilizing the measurements [19]. The constant ambient temperature boundary condition is set to the structure backside supposing ideal heat transfer between leadframe and heatsink. The structure self-heating is simulated by three thermal contacts placed along 2DEG between drain and source corresponding to the dissipated power source located: 1) along drain to source access region; 2) region under the gate electrode; and 3) pinch-off region located at the drain side gate edge [20]. The material thermal coefficients for the structure model and thermal boundary resistance (TBR) of the interfaces were taken from the literature and subsequently calibrated using infrared imaging measurement and micro-Raman thermometry [20].

TABLE I
THERMAL COEFFICIENTS

Material	Thermal conductivity ($\mathrm{W.m^{-1}K^{-1}}$)
Au	310
AlGaN	$40.(T/298)^{1.37}$
GaN (C doped)	$190.(T/298)^{1.37}$
4H-SiC xy-axis	$430.(T/298)^{1.5}$
z-axis	$370.(T/298)^{1.5}$
AuSn	57
CuMo	160

The thermal coefficients for the FEM simulation are in Table I. The TBR is set to 1×10^4 $\mathrm{cm^2KW^{-1}}$ at the GaN/SiC interface. TBR value of 2 $\mathrm{cm^2KW^{-1}}$ is set at the CuMo leadframe/cooler interface. The cooler temperature is set to a constant ambient temperature. It represents an ideal heatsink.

B. Trapping Phenomena Determination

The short-pulsed, long-pulsed, or quasi-static transfer $I - V$ characteristics measured at the same T_{0L} and V_{DS} are assumed pointing on the same threshold voltage V_{TH} independent on V_{GS} for the trapping free device. Therefore, V_{TH} shift gives opportunity to incorporate time dependent isothermal trapping phenomena under the gate to determine T_A [13].

To acquire $V_{\mathrm{TH}}(t \rightarrow 0, T_{0L})$ and isothermal transconductance $g_{M0}(T_{0L})$, pulsed transfer $I - V$ characteristics of pulselength ~100 ns, constant amplitude $V_{\mathrm{DS}} = 2$, 20 V, sweeping amplitude V_{GS} in the range −4 to 0 V, and T_{0L} range 25 °C–185 °C were measured.

The I_{DS} time response was acquired using a combined V_{DS} and V_{GS} pulse of length ~1 s with a constant amplitude $V_{\mathrm{DS}} = 2$, 20 V, and a stepping amplitude V_{GS} in the range −4 to −1 V. This makes possible to approximate $V_{\mathrm{TH}}(t, T_{0L})$ for t step of one decade and T_{0L} step ~20 °C. Thus, it is possible to obtain t and T_{0L} dependent trapped charge isothermal current variation $\Delta I_{\mathrm{TE}}(t, T_{0L}) = -g_{M0}(T_{0L})[V_{\mathrm{TH}}(t, T_{0L}) - V_{\mathrm{TH}}(t \rightarrow 0, T_{0L})]$.

C. Thermal Resistance Determination

The I_{DS} time dependence for voltage pulse of amplitude $V_{\mathrm{DS}} \approx 2$ V, $V_{\mathrm{GS}} = 0$ V and length $t_S \approx 1$ s was measured at

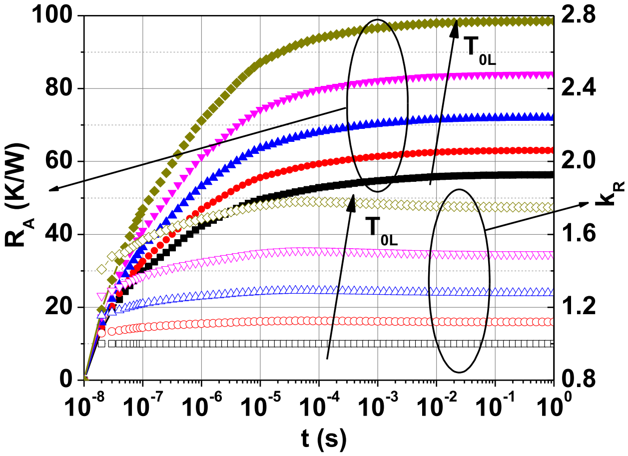

Fig. 3. Thermal impedance R_A and normalized thermal resistance k_R time dependence for T_{0L} in the range of 25 °C–185 °C (40 °C step).

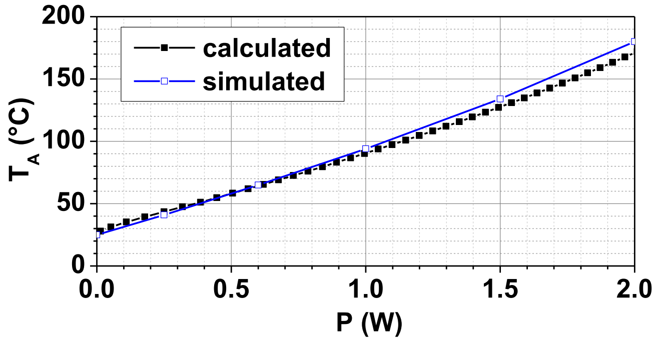

Fig. 4. Simulated and calculated average temperature T_A versus dissipated power in the quasi-static state.

varying ambient temperature T_{0L} in the range of 25 °C–185 °C with the step ~20 °C as depicted in Fig. 1. Then I_{DS} approximation for 20 ns $< t <$ 60 ns by exponential function results in $t_D \approx 5$ ns calculated by (A1) utilizing $t_1 \approx 20$ ns and I_{D0} estimation by (A2) gives opportunity to plot $I_{D0} + \Delta I_{\mathrm{TE}}$ time dependence shown in Fig. 1.

The dependence of the measured current I_{DS} acquired at $t \approx 1$ s equivalent to the quasi-static state on the ambient temperature and the estimated initial current I_{D0} at $V_{\mathrm{DS}} =$ 2 V is shown in Fig. 2. The term ΔI_{TE} exhibits ~2%–4% of the term $I_{\mathrm{DS}} - I_{D0}$ under low-power operation.

Subsequently $R_A(t, T_{0L})$ is calculated utilizing (1) and shifted by $t_D \approx 5$ ns is shown in Fig. 3. For T_A determination under high-power operation at ambient temperature $T_{0H} \approx$ 25 °C, $R_A(t, T_{0L})$ is normalized utilizing time-dependent $k_R = R_A(t, T_{0L})/R_A(t, T_{0H})$ as depicted in Fig. 3.

D. Average Temperature Determination With Direct Use of Thermal Resistance

Utilizing $R_{A\infty}(T_{A,k})$ obtained by (1) in recurrent calculations (3) results in average temperature determination in the quasi-static state as depicted in Fig. 4.

The dissipated power time dependence $P(t)$ was calculated from I_{DS} and V_{DS} time response at $T_{0H} \approx$ 25 °C shown in Fig. 5. Employing $t_1 \approx 70$ ns in (A1) results in $t_D \approx 17$ ns and $T_A(t_1)$ was estimated by (A4). Subsequently, T_A recurrent calculations (4) utilizing $R_A(t_k, T_{A,k})$ obtained from Fig. 3 shifted by $t_D \approx 17$ ns were applied to obtain T_A time dependence as shown in Fig. 6.

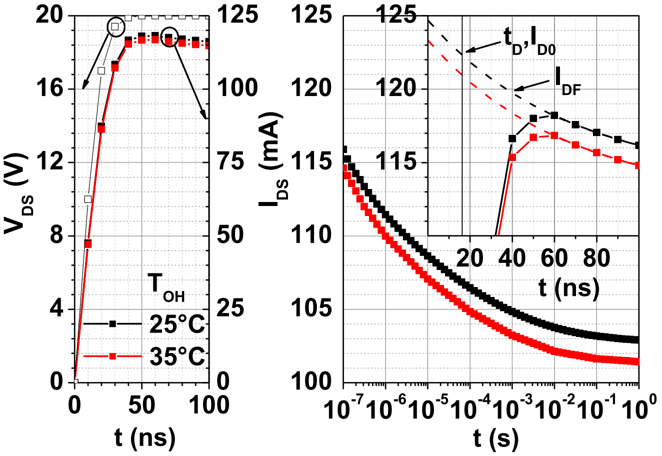

Fig. 5. Short-time V_{DS}, I_{DS}, and logarithmic I_{DS} time dependence. (Inset: magnified I_{DS} at $V_{\mathrm{DS}} = 20$ V.)

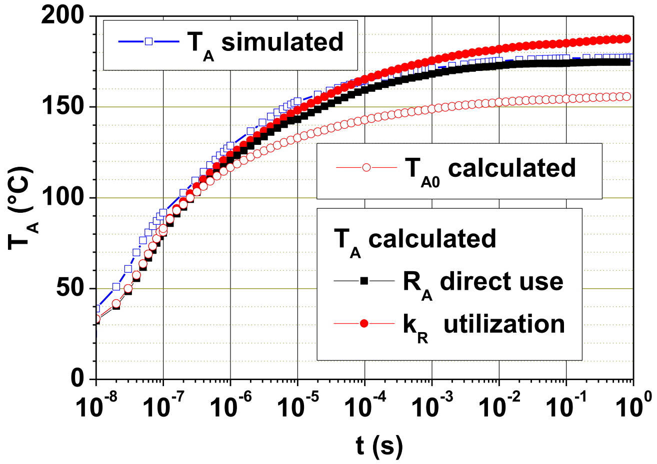

Fig. 6. Simulated and calculated average temperature T_A and T_{A0} versus time for pulsed operation.

To compare calculated and simulated results, the source-to-gate serial resistance is supposed as the main thermal parameter for the HEMT [9]. The simulated average channel temperature of the source to the gate area is assumed as T_A. A good T_A correspondence with numerical simulations points on the small deviation between $R_A(t, T_{0L})$ and $R_A(t, T_A)$ utilized in the linear and saturation regime, respectively.

E. Average Temperature Determination Utilizing Normalized Thermal Resistance

The application of the method introduced in theoretical Section III-C is described below. The pulse $V_{\mathrm{DS}} \approx 20$ V of length $t_S \sim 1$ s for gate–source voltage $V_{\mathrm{GS}} = 0$ V at ambient temperature $T_{0H} \approx$ 25 °C and $T_{0H} + \Delta T_{0H} \approx$ 35 °C was applied and I_{DS} time response was acquired as depicted in Fig. 5 giving opportunity to determine ΔI^*_{DS}.

Fitting of I_{DS} by exponential function in the range 70 ns $< t <$ 200 ns results in $t_D \approx 17$ ns and I_{D0} estimation utilizing (A1) and (A2), respectively, taking high-power operation V_{DS} and I_{DS} rising time emphasized in Fig. 5 into account. Subsequently, T_A at $t_1 \approx 70$ ns was obtained utilizing (A3) as initial condition for recurrent calculations.

The acquired $\Delta I_{TE}(t, T_{0L})$ dependence in experimental Section III-B allows to incorporate the isothermal trapping process under high-power operation at operating temperature $T_A = T_{0L}$ by the term $dI_{\mathrm{TE}}(t, T_{0L}) \approx \Delta I_{\mathrm{TE}}(t + dt, T_{0L}) - \Delta I_{\mathrm{TE}}(t, T_{0L})$ incorporated in $dI_T(t) = dI_{\mathrm{DS}}(t) - dI_{\mathrm{TE}}(t, T_A)$ in (5).

Recurrent calculations utilizing k_R depicted in Fig. 3 shifted by $t_D \approx 17$ ns were applied to obtain T_A time dependence as shown in Fig. 6 exhibiting a good correspondence with results obtained by device thermal simulation for investigated $\mathrm{Al_{0.25}Ga_{0.75}N/GaN}$ HEMT. The value T_{A0} calculated by (5) is k_R independent and useful for $R_A(t, T_{OH})$ comparison under low-power and high-power operation. Relative k_R time variation is lower than relative R_A variation, especially at the pulse beginning, hence incorrect t_D determination under low-power operation is less considerable compared to method employing low-power operation R_A directly. At the pulse beginning R_A is determined mainly by elementary thermal capacitance combination whereas at the end of the pulse by elementary thermal resistance combination.

IV. CONCLUSION

The average channel temperature of the AlGaN/GaN HEMT under high-performance operation was determined using a modified device thermal model in pulsed and quasi-static operating mode. This was achieved by a differential analysis employing the isothermal and thermal part of the resulting current. The key advantages of the proposed method are as follows: 1) isothermal trapping phenomena are incorporated utilizing threshold voltage shift and transconductance; 2) device thermal stress suppression by the ambient temperature increase under the low-power operation only; and 3) self-heating process at the beginning of the pulse during the rising edge obtained from the time dependence of voltage and current was discussed and analyzed in the appendix. Thermal resistance calculated from low-power operation was directly utilized in high-power average temperature recurrent calculations. The normalized thermal resistance obtained from low-power operation was utilized to calculate the HEMT average channel temperature under high-power operation. Both methods were compared and discussed exhibiting a good correspondence with numerical simulations. The average temperature ~175 °C was calculated at the end of dissipated power pulse ~2 W when the device quasi-static state was reached. Significantly reduced thermal stress during measurements makes this method applicable for vulnerable devices.

APPENDIX

After rectangular V_{GS} or V_{DS} pulse is applied at the zero time and ambient temperature $T_0 = T_{0L}$ or $T_0 = T_{0H}$, the time t_1 is required for charging device parasitic electric capacitance and free carrier filling. This results in variable dissipated power $P(t) = V_{\mathrm{DS}}(t)I_{\mathrm{DS}}(t)$ and eligible T_A increase [13]. However, in the short time interval $t_1 < t < t_2$ in the same order as t_1, due to negligible charge trapping and small $P(t)$ variation, I_{DS} is possible to be approximated by fitting function $I_{\mathrm{DF}}(t)$ linearly dependent on T_A. For $t < t_2$, T_A is supposed to be increased by heat flux linearly dependent on $P(t)$ due to thermal capacitance charging major role.

To reach the same T_A at t_1 for real pulse including parasitic capacitance and increasing $P(t)$ and ideal pulse containing zero V_{DS} and I_{DS} rising time and $P(t) \approx P(t_1)$ for $t_D < t < t_1$, the ideal pulse is required to be delayed by t_D meeting the requirement $\int_0^{t_1} P(t)dt = \int_{t_D}^{t_1} V_{\mathrm{DS}}I_{\mathrm{DF}}(t)dt$. Negligible $V_{\mathrm{DS}}I_{\mathrm{DF}}(t)$ variation in comparison to real $P(t)$ for $t < t_1$ results in

$$t_D = t_1 - P^{-1}(t_1)\int_0^{t_1} P(t)dt \tag{A1}$$

$$I_{D0} = I_{\mathrm{DF}}(t_D). \tag{A2}$$

The device investigated at two ambient temperatures T_0, $T_0 + \Delta T_0$ of relatively small difference ΔT_0 gives opportunity to calculate $\Delta T_A(t_1) = T_A(t_1) - T_0$ valid for low-power as well as high-power operation coming out from (1)

$$\Delta T_A(t_1) = \Delta T_0 I_{\mathrm{DS}}(t_1)[I_{\mathrm{DS}}(t_1) - I_{D0}]/\big[I_{D0}\Delta I^*_{\mathrm{DS}}(t_1)\big]. \tag{A3}$$

Already known $R_A(t, T_0)$ for the ideal V_{DS} and I_{DS} pulse gives opportunity to calculate $\Delta T_A(t_1)$ for real pulse

$$\Delta T_A(t_1) = P(t_1)[dR_A(t_1 - t_D, T_0)/dt][t_1 - t_D]. \tag{A4}$$

The value $T_A(t_1)$ is advised to be utilized as the initial condition for recurrent calculations. Subsequently, $R_A(t, T_{0L})$ and $k_R(t, T_{0L})$ obtained from low-power operation measurements are required to be shifted by t_D to be employed in high-power operation calculations.

The I_{D0} and $T_A(t_1)$ estimation brings more accurate results for widely utilized standard methods based on isothermal and real resultant current comparison.

ACKNOWLEDGMENT

The JU receives support from the European Union's Horizon 2020 Research and Innovation Program and France, Germany, Slovakia, Netherlands, Sweden, Italy, Luxembourg, and Ireland. This publication reflects only the author's view and the JU is not responsible for any use that may be made of the information it contains.

REFERENCES

[1] O. Ambacher *et al.*, "Two-dimensional electron gases induced by spontaneous and piezoelectric polarization charges in N- and Ga-face AlGaN/GaN heterostructures," *J. Appl. Phys.*, vol. 85, no. 6, p. 3222, Mar. 1999, doi: 10.1063/1.369664.

[2] M. K. Chattopadhyay and S. Tokekar, "Thermal model for DC characteristics of AlGaN/GaN HEMTs including self-heating effect and non-linear polarization," *Microelectron. J.*, vol. 39, pp. 1181–1188, Oct. 2008, doi: 10.1016/j.mejo.2008.01.043.

[3] A. Nigam, T. N. Bhat, S. Rajamani, S. B. Dolmanan, S. Tripathy, and M. Kumar, "Effect of self-heating on electrical characteristics of AlGaN/GaN HEMT on Si (111) substrate," *AIP Adv.*, vol. 7, no. 8, Oct. 2008, Art. no. 085015, doi: 10.1063/1.4990868.

[4] S. Chowdhury, "Gallium nitride based power switches for next generation of power conversion," *Phys. Status Solidi A*, vol. 212, pp. 1066–1074, May 2015, doi: 10.1002/pssa.201431810.

[5] M. Östling, R. Ghandi, and C.-M. Zetterling, "SiC power devices—Present status, applications and future perspective," in *Proc. 23rd Int. Symp. Power Semiconductor Devices IC's*, San Diego, CA, USA, May 2011, pp. 10–15, doi: 10.1109/ISPSD.2011.5890778.

[6] K. J. Chen *et al.*, "GaN-on-Si power technology: Devices and applications," *IEEE Trans. Electron Devices*, vol. 64, no. 3, pp. 779–794, Mar. 2017, doi: 10.1109/TED.2017.2657579.

[7] F. Berthet *et al.*, "Characterization of the self-heating of AlGaN/GaN HEMTs during an electrical stress by using Raman spectroscopy," *Microelectron. Rel.*, vol. 51, nos. 9–11, pp. 1796–1800, Sep. 2011, doi: 10.1016/j.microrel.2011.07.022.

[8] J. Kim *et al.*, "Effective temperature measurements of AlGaN/GaN-based HEMT under various load lines using micro-Raman technique," *Solid-State Electron.*, vol. 50, no. 3, pp. 408–411, Mar. 2006, doi: 10.1016/j.sse.2005.11.009.

[9] J. Kuzmík, P. Javorka, A. Alam, M. Marso, M. Heuken, and P. Kordoš, "Determination of channel temperature in AlGaN/GaN HEMTs grown on sapphire and silicon substrates using DC characterization method," *IEEE Trans. Electron Devices*, vol. 49, no. 8, pp. 1496–1498, Aug. 2002, doi: 10.1109/TED.2002.801430.

[10] R. Menozzi *et al.*, "Temperature-dependent characterization of AlGaN/GaN HEMTs: Thermal and source/drain resistances," *IEEE Trans. Device Mater. Rel.*, vol. 8, no. 2, pp. 255–264, Jun. 2008, doi: 10.1109/TDMR.2008.918960.

[11] T. S. Tarter, "A novel circuit for the evaluation of thermal impedance characteristics of MOS integrated circuits," in *Proc. IEEE Semiconductor Thermal Temp. Meas. Symp. (SEMI-THERM)*, San Diego, CA, USA, Feb. 1989, pp. 131–135, doi: 10.1109/STHERM.1989.76078.

[12] B. Raj and S. Bindra, "Thermal analysis of AlGaN/GaN HEMT: Measurement and analytical modeling techniques," *Int. J. Comput. Appl.*, vol. 75, no. 18, pp. 1–10, Aug. 2013, doi: 10.5120/13346-9922.

[13] M. Florovič, J. Kováč, A. Chvála, J. Kováč, J.-C. Jacquet, and S. L. Delage, "Theoretical and experimental substractions of device temperature determination utilizing I–V characterization applied on AlGaN/GaN HEMT," *Electronics*, vol. 10, no. 22, p. 2738, Nov. 2021, doi: 10.3390/electronics10222738.

[14] M. A. Alim, A. A. Rezazadeh, and C. Gaquiere, "Temperature dependence of the threshold voltage of AlGaN/GaN/SiC high electron mobility transistors," *Semicond. Sci. Technol.*, vol. 31, no. 12, Nov. 2016, Art. no. 125016, doi: 10.1088/0268-1242/31/12/125016.

[15] M. Florovič *et al.*, "Models for the self-heating evaluation of a gallium nitride-based high electron mobility transistor," *Semicond. Sci. Technol.*, vol. 36, no. 2, Jan. 2021, Art. no. 025019, doi: 10.1088/1361-6641/abd15a.

[16] M. Florovič *et al.*, "AlGaN/GaN HEMT channel temperature determination utilizing external heater," *Semicond. Sci. Technol.*, vol. 35, no. 2, Feb. 2020, Art. no. 025006, doi: 10.1088/1361-6641/ab5d85.

[17] M. Florovic *et al.*, "Rigorous channel temperature analysis verified for InAlN/AlN/GaN HEMT," *Semicond. Sci. Technol.*, vol. 34, May 2019, Art. no. 065021, doi: 10.1088/1361-6641/ab1737.

[18] *Sentaurus Device User Guide, Version L-2017.09*, Synopsys TCAD Sentaurus, San Jose, CA, USA, 2017.

[19] A. Chvála *et al.*, "Analysis of multifinger power HEMTs supported by effective 3-D device electrothermal simulation," *Microelectron. Rel.*, vol. 78, pp. 148–155, Nov. 2017, doi: 10.1016/j.microrel.2017.08.012.

[20] A. Chvála *et al.*, "Advanced characterization techniques and analysis of thermal properties of AlGaN/GaN multifinger power HEMTs on SiC substrate supported by three-dimensional simulation," *J. Electron. Packag.*, vol. 141, no. 3, May 2019, Art. no. 031007, doi: 10.1115/1.4043477.